ARL-TR-7782 ● SEP 2016

US Army Research Laboratory

Change in Weather Research and Forecasting (WRF) Model Accuracy with Age of Input Data from the Global Forecast System (GFS)

by JL Cogan

NOTICES

Disclaimers

The findings in this report are not to be construed as an official Department of the Army position unless so designated by other authorized documents.

Citation of manufacturer's or trade names does not constitute an official endorsement or approval of the use thereof.

Destroy this report when it is no longer needed. Do not return it to the originator.

ARL-TR-7782 ● SEP 2016

US Army Research Laboratory

Change in Weather Research and Forecasting (WRF) Model Accuracy with Age of Input Data from the Global Forecast System (GFS)

by JL Cogan
Computational and Information Sciences Directorate, ARL

REPORT DOCUMENTATION PAGE

Form Approved
OMB No. 0704-0188

1. REPORT DATE *(DD-MM-YYYY)*	2. REPORT TYPE	3. DATES COVERED (From - To)
September 2016	Technical Report	April 2016–July 2016

4. TITLE AND SUBTITLE
Change in Weather Research and Forecasting (WRF) Model Accuracy with Age of Input Data from the Global Forecast System (GFS)

5a. CONTRACT NUMBER

5b. GRANT NUMBER

5c. PROGRAM ELEMENT NUMBER

6. AUTHOR(S)
JL Cogan

5d. PROJECT NUMBER

5e. TASK NUMBER

5f. WORK UNIT NUMBER

7. PERFORMING ORGANIZATION NAME(S) AND ADDRESS(ES)
US Army Research Laboratory
ATTN: RDRL-CIE
2800 Powder Mill Road
Adelphi, MD 20783-1138

8. PERFORMING ORGANIZATION REPORT NUMBER
ARL-TR-7782

9. SPONSORING/MONITORING AGENCY NAME(S) AND ADDRESS(ES)

10. SPONSOR/MONITOR'S ACRONYM(S)

11. SPONSOR/MONITOR'S REPORT NUMBER(S)

12. DISTRIBUTION/AVAILABILITY STATEMENT
Approved for public release; distribution unlimited.

13. SUPPLEMENTARY NOTES

14. ABSTRACT
Mesoscale models generate output for many applications worldwide. Normally, initialization of a mesoscale model employs the most recent output available from a larger-scale regional or global model. Such output also is used to adjust the lateral boundary conditions as the larger-scale model evolves. However, some applications, especially in remote or minimally connected areas, may require the use of large-scale model data that may be one or more days old. The analysis of this report investigates the effect of using older large-scale data on mesoscale model accuracy. The report briefly describes the procedure and presents the results of a preliminary analysis. As expected, accuracy generally tended to decline as the large-scale data aged, but appeared to improve slightly as the age of the large-scale data increased from 3 days old to 4 days old. Also, there is a wide variation between individual cases. The change in meteorological variables is explored, but the emphasis is on the effect on simulated artillery trajectories. The use of trajectories with their major dependence on meteorological conditions provides a means to check the net overall ability of a model to simulate the atmosphere over the space and time covered by the trajectory.

15. SUBJECT TERMS
WRF, Weather Research and Forecasting, accuracy, aged GFS on WRF accuracy, Global Forecast System

16. SECURITY CLASSIFICATION OF:			17. LIMITATION OF ABSTRACT	18. NUMBER OF PAGES	19a. NAME OF RESPONSIBLE PERSON
a. REPORT	b. ABSTRACT	c. THIS PAGE			19b. TELEPHONE NUMBER (Include area code)
Unclassified	Unclassified	Unclassified	UU	44	James L Cogan 301-394-2304

Standard Form 298 (Rev. 8/98)
Prescribed by ANSI Std. Z39.18

Contents

List of Figures

List of Tables

1. Introduction

Mesoscale models, such as the Weather Research and Forecasting (WRF) model (http://wrf-model.org/wrfadmin/publications.php), generate output for many applications worldwide that include, but are not limited to, regional forecasts for civilian and military operations and planning; research such as for aerosol distribution and transport; and other uses for Government, agriculture, and industry. Normally, initialization of a mesoscale model employs the most recent output available from a larger-scale regional or global model, such as the National Centers for Environmental Prediction's Global Forecast System (GFS; http://www.ncdc.noaa.gov/data-access/model-data/model-datasets/global-forcast-system-gfs) or the US Air Force's Global Air Land Weather Exploitation Model, a version of the United Kingdom's Unified Model (http://www.metoffice.gov.uk/research/modelling-systems/unified-model).

The GFS, or another large-scale model, is also used to adjust the lateral boundary conditions during the forecast period of the mesoscale model as the larger-scale model evolves over time. However, some applications, especially in remote or other areas with minimal or no connectivity to sources of data, may require the use of large-scale model data that may be one or more days old. First responders to an emergency in a remote area may not have sufficient access to the Internet or other means of obtaining large-scale model data. First-in military forces may not have access to reachback for several days or severe limitations may result in communication of only the very highest priority messages.

Some meteorological centers compare global and large-scale regional model meteorological output versus radiosonde observation (RAOB) data more or less continuously and some make intermodel comparisons. The National Center for Environmental Prediction (NCEP) (http://www.emc.ncep.noaa.gov/gmb/STATS_vsdb/) and the European Centre for Medium-Range Weather Forecasting (ECMWF) (http://www.ecmwf.int/en/forecasts/charts/medium/monthly-wmo-scores-against-radiosondes) have readily accessible websites. Worldwide comparisons are available for deterministic forecasts at http://apps.ecmwf.int/wmolcdnv/ and for ensemble forecasts at the Japan Meteorological Agency at (http://epsv.kishou.go.jp/EPSv/). These sites provide comparisons of meteorological variables at the standard World Meteorological Organization (WMO) pressure levels (e.g., 850, 700, and 500 hPa), and the ECMWF site presents graphs showing the change in global model accuracy with time starting at 24 h of model time up to as much as 240 h for a subset of the models compared. Various organizations display WRF output, especially in graphical formats. Examples include the National Center for Atmospheric Research (NCAR) at http://wrf-

model.org/plots/realtime_main.php, NCEP at http://mag.ncep.noaa.gov/model-guidance-model-area.php#, and the Earth System Research Laboratory (ESRL) of the National Oceanic and Atmospheric Administration (NOAA) at http://rapidrefresh.noaa.gov/. However, they do not have readily available sites showing the change in accuracy of WRF output relative to observations as the large-scale data age.

In addition, several investigators have compared WRF output against radiosonde data as part of their experiments or evaluations. For example, Schroeder et al. (2006) compared data from the older Mesoscale Model Fifth Generation over its vertical extent and presented results for standard pressure levels from 850 to 100 hPa (some graphs to 150 hPa). They worked with data for 8 days in April 2002, 12 days in winter and summer 2003, and 18 days in August 2001. The former 2 periods were from the East Coast region of the United States and the latter from the Great Plains region of the United States. Kilpelainen et al. (2012) and Dutsch (2012) each evaluated WRF output for the boundary layer over Svalbard in the Arctic in terms of height above ground compared to tower and tethered balloon (tethersonde) data and radiosonde data, respectively. The tethersondes provided data from the surface up to about 600, 800, and 1,250 m for each of 3 sites, respectively. The radiosonde data reached as high as 2 km above the surface. However, none of these investigations apparently considered the effect of the use of older GFS or other large-scale model data on the output of WRF or other mesoscale model.

The analysis in the present report investigated the effect on the accuracy of WRF as a representative mesoscale model when using older large-scale data (i.e., from GFS). Skamarock et al. (2008) describe the basic features of WRF (although the model has evolved since). The present report briefly describes the analysis procedure and presents preliminary results. As expected, accuracy generally tended to decline as the large-scale data aged, but appeared to slightly increase from 3 days old to 4 days old. Also, there was a wide variation in accuracy between individual cases. The change in the meteorological variables was examined, but the primary emphasis concerned the effect on the radial miss distances (RMDs) derived from simulated artillery trajectories computed using the General Trajectory (GTRAJ) model from the US Army Armaments Research Development and Engineering Center (ARDEC). The use of trajectories, with their major dependence on meteorological conditions, provides a means to check the net overall ability of a model to simulate the atmosphere as an integrated whole over the space and time covered by the trajectory. The Computer Meteorological Message (METCM), commonly used for accounting for meteorological effects in artillery trajectory calculations, provided the meteorological data required by GTRAJ.

2. Data

The METCM consists of meteorological data (i.e., pressure, virtual temperature, wind speed, and wind direction) for the surface and a series of vertical layers, extending up to 30 km above ground level (AGL), also known as METCM zones. STANAG 4061 (2000) describes the METCM in greater detail. For the current study, METCMs were derived from both WRF-based profiles and RAOB soundings. The generation of vertical profiles of meteorological variables for the METCM is based on algorithms implemented in software described in Cogan (2015). That software package processes either model data or RAOB soundings into a variety of message type including the METCM. Vertical profiles were extracted from WRF Network Common Data Form output files via a NCAR Command Language (NCL) script using a method developed by Reen (2015). The profiles were placed into text files that included a header with information on the location, time, model grid resolution, and method (if any) employed to interpolate between model grid points to the selected location. These profiles contain data lines for heights above mean sea level (MSL) of pressure levels. The user has the option to use a "sounding" from the nearest grid point (i.e., no interpolation), or either bilinear interpolation or inverse distance weight interpolation (via built-in NCL capabilities). RAOB data were downloaded from the University of Wyoming's weather website (http://www.weather.uwyo.edu/upperair/sounding.html). An alternative site is the RAOB archive hosted by the NOAA ESRL at their website (http://www.esrl.noaa.gov/raobs/).

WRF v3.7.1 was run with 9-, 3-, and 1-km horizontal grid spacing nested domains. The comparisons for this report used data from the 3-km domain. The initial and boundary conditions were derived from GFS 0.5° horizontal grid spacing with a 3-h time interval. Where available, GFS snow fields were replaced with 1-km snow fields from the National Weather Service's National Operational Hydrologic Remote Sensing Center (NOHRSC) (http://www.nohrsc.noaa.gov/technology/) Snow Data Assimilation System, or if not available, with 4-km snow cover fields from the National Ice Center's Interactive Multi-sensor Snow and Ice Mapping System (IMS) (http://nsidc.org/data/docs/noaa/ g02156_ims_snow_ice_analysis/). Consequently, when available, NOHRSC fields were used for an area centered on the United States, IMS data for the rest of the northern hemisphere, and GFS fields for the southern hemisphere. A sea surface temperature product with higher resolution than the GFS output is produced by NCEP's Marine Modeling and Analysis Branch, called the Real-Time Global Sea Surface Temperature (Gemmill et al. 2007), which has 1/12th-degree horizontal grid spacing and was used to specify sea surface temperatures. These WRF runs did not use data assimilation (i.e., observation "nudging") in order to simulate the conditions that could occur if

operating in a remote area without adequate connection to a source of external data. If we assume observation data were available at the start of the initial period (e.g., prior to leaving a home location), but not afterwards, any noticeable effect on the model calculations would have ended prior to the 12-h forecast of the first run. The Mellor-Yamada-Janjić scheme is used to parameterize the atmospheric boundary layer. As in Lee et al. (2012) and Reen et al. (2014), the background turbulent kinetic energy is decreased to better simulate conditions with low turbulent kinetic energy and the atmospheric boundary layer depth diagnosis is altered. The WRF single-moment, 5-class microphysics parameterization and the Kain-Fritsch cumulus parameterization (9-km domain only) are used. For radiation, the Rapid Radiative Transfer Model is used for longwave and the Dudhia scheme for shortwave. The Noah land surface model is used to represent land surface processes.

The selected RAOB sites cover various regions and seasons in the northern and southern hemispheres. Table 1 presents a list of regions with the included WMO sites and the date and time of the WMO RAOBs. Analysis locations were selected using locations from previous investigations and tests, which helped ensure availability of data from WMO RAOB sites. To reduce the number of model runs and reduce analysis time, groups of WMO sites were sought that fit within the bounds of the middle WRF nest or domain. The horizontal grid resolution of the middle nest (3 km) is similar to current and near-term planned resolutions used in operational meteorological systems. For some regions, up to 5 sites fit within the bounds of the 3-km domain (723 x 723 km), allowing for sufficient distance from the lateral boundaries to avoid unwanted effects that potentially could arise from the different grid resolutions of the outer and middle domains (9 and 3 km). That distance is generally considered to be on the order of 20 to 30 (or more) grid points, or, in this case, about 60 to 90 km. That leaves a central region no less than about 540 × 540 km (~180 × 180 grid points). The exception was San Diego, California, which was only about 10 to 11 grid points from the edge of the domain. However, the results seemed in line with, or even better, than from the other sites within the "Southwest" region. In some regions, as in the southern hemisphere, only 2 sites fit within the middle domain. Data were extracted for all seasons but mostly for winter and spring and mostly for regions within the United States. A total of 50 cases were examined where each case contains comparisons between a METCM derived from a RAOB with 5 METCMs derived from the 5 runs of WRF (one for each GFS "age" used for initialization).

Table 1 RAOB sites and WMO identifiers, when available, are listed; otherwise, the first 3 or 4 letters of the site's name are used (e.g., MEIN for Meiningen). Each site has the respective dates and times for a total of 50 cases. Latitude and longitude of the center of each WRF domain used for the listed region are shown. Here Midwest applies to several sites within the region often called the "southern plains". East Coast refers to locations along or near the center of the eastern coast of the United States. US regions are listed first followed by several international regions.

Region	Site	ID	Date and Time (yyyy-mm-dd-hh)	Center Lat, Lon (degrees)
Alaska US	Anchorage	PANC	2016-01-11-00	59.46, –153.34
	King Salmon	PAKN	and	
	Kodiak	PADQ	2016-04-06-12	
East Coast US	Blacksburg, VA	RNK	2016-03-23-00	36.88, –77.94
	Dulles Int'l AP, VA	IAD	and	
	Greensboro, NC	GSO	2016-05-19-12	
	Newport, NC	MHX		
	Wallops Is., VA	WAL		
Midwest US	Amarillo, TX	AMA	2016-01-02-12	37.12, –98.66
	Dodge City, KS	DDC	and	
	Lamont, OK	LMN	2016-02-10-12	
	Norman, OK	OUN		
	Topeka, KS	TOP		
Southwest US	Flagstaff, AZ	FGZ	2016-06-18-12	33.78, –113.57
	Las Vegas, NV	VEF		
	Phoenix, AZ	PHX		
	San Diego, CA	NKX		
	Tucson, AZ	TUS		
Australia	Adelaide	YPAD	2016-05-05-12	–36.05, 141.69
	Melbourne	YMML		
Germany	Bergan	ETGB	2016-02-07-00	50.82, 9.62
	Idar-Oberstein	ETGI	and	
	Kuemmersbruck	ETGK	2016-03-07-00	
	Meiningen	MEIN		
	Stuttgart	STUT		

Table 1 RAOB sites and WMO identifiers (continued)

Region	Site	ID	Date and Time (yyyy-mm-dd-hh)	Center Lat, Lon (degrees)
South Africa	King Shaka	FALE	2016-05-06-00	–27.76, 29.66
	Pretoria	FAIR		
South Korea	Cheju	CHEJ	2015-11-07-12	35.19, 127.42
	Heuksando	HEUK		
	Kwangju	RKJJ		
	Osan Air Base	RKSO		
	Pohang	POHA		

Though a rare occurrence, the main NOAA archive used for the 0.5° data (https://catalog.data.gov/dataset/global-forecast-system-gfs-0-5-deg) occasionally omits some GFS output. Unfortunately, one such event meant that Day–4 GFS data were not available for the first of 2 Midwest US groups listed in Table 1 (2016-01-02-12). However, the data were available via an alternate website that contains GFS output for 0.5° and 1.0° grids, (http://www.ncdc.noaa.gov/has/HAS.FileAppRouter?datasetname=GFS3&subqueryby=STATION&applname=&outdest=FILE).

3. Procedure

The WRF was run to produce 12-h forecasts that ended at the time of the respective coincident RAOB. It was initialized using 0.5° GFS data starting with the GFS 0-h forecast and working backwards, and the GFS data were used to update the WRF boundary conditions. Therefore, the WRF 0-h forecast time was the same as the GFS time for a 0-, 24-, 48-, 72-, or 96-h forecast from the same day, 1, 2, 3, or 4 days earlier, respectively. For example, for a 12 Coordinated Universal Time (UTC) RAOB on 25 March, GFS forecast data were obtained every 3 h from the 00 UTC, 25 March data set. In this example, the WRF-based sounding was extracted from the 12-h WRF data so as to match the RAOB time. This procedure was repeated using GFS data from progressively older GFS runs one day apart. For example, the 2-day-old GFS data started on 00 UTC, 23 March. WRF would be run again for 00 UTC, 25 March, but using data from the 2-day-old GFS data set to produce the sounding 12 model hours later than was used to generate the respective METCM. Consequently, WRF soundings were extracted to compare with the same RAOB, but initialized using GFS data that began 0, 24, 48, 72, and 96 h earlier. Figure 1 illustrates the scheme employed to obtain the “aged” GFS data. In the figure, the circles at the left of each line indicate the GFS start time. The WRF start

times relative to the GFS start time (0-h forecast) are shown along the solid vertical line (left), and the times of the WRF 12-h forecast and coincident RAOB are shown along the vertical dashed line (right).

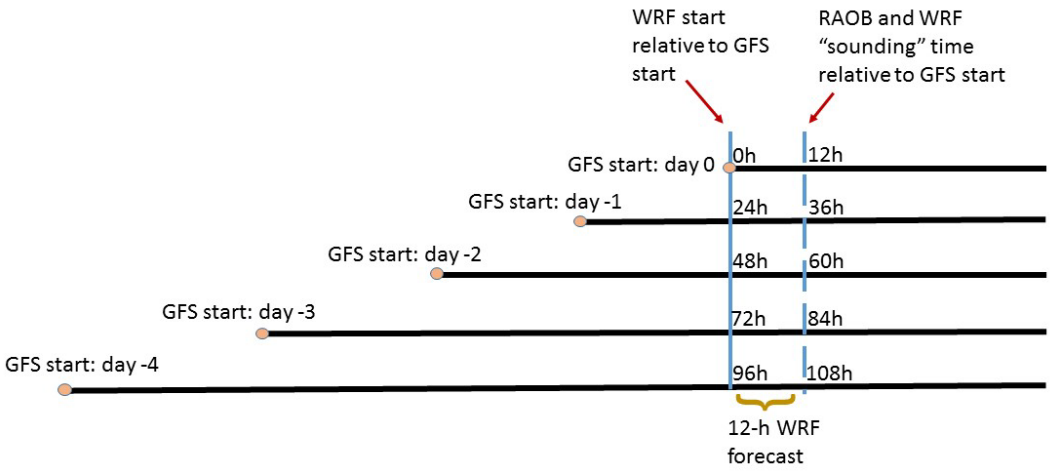

Fig. 1 Scheme employed to obtain GFS data for use with WRF. The circles at the left end of the horizontal lines indicate the time of start of the GFS data for each day.

This method uses successive GFS data sets as input to the WRF model forecasts used to produce soundings contemporaneous to an actual RAOB used as an approximation to truth.

Use of this method to obtain the older GFS data eliminated the potential effect of changes in meteorological conditions that would occur if a single GFS data set was used along with sequential RAOBs. An example is a set of GFS files for 2016032500 with WRF soundings and RAOBs at 12 UTC on 25, 26, 27, 28, and 29 March. During that period of 5 days, the RAOBs would reflect the actual changes in the weather and consequently could be confused with changes in the WRF output arising from the use of older GFS data. Therefore, it would be difficult to separate the effect of the aging GFS from the effect of the actual change in the weather.

The next step was the preprocessing on a local computer of the GFS data for the selected period and location using scripts developed by Reen (2015) that included modifications that corrected some deficiencies in the original code. This preprocessing step converts the GFS and other data (including observations when available with data assimilation activated) into forms appropriate for input to the WRF model itself. The resultant preprocessed files were transferred to a high-performance computer (HPC) since the HPC could run multiple instances of WRF in a much shorter time. The WRF output files for the 3-km grid domain were

transferred back to the local computer for generation of the meteorological profiles. Vertical profiles were extracted from the WRF output files via an NCL script. The RAOB and WRF profiles were placed into text files and transferred to a local Windows desktop for conversion into text file "messages" that have the data in the same units and structure as in the METCM. Cogan (2015) describe the program for conversion of RAOB or WRF soundings into METCMs and various other types of meteorological messages. This program also produces a form of the METCM that is suitable for input to the GTRAJ trajectory simulation program. That format also is convenient for use in spreadsheets employed for the meteorological comparisons of this report.

The meteorological values of the METCM, that is, pressure, virtual temperature, wind speed, and wind direction, plus some derived variables such as density, were compared using spreadsheets similar to those in Cogan (2015) for METCM zones up through zone 26 (19–20 km), which is the highest zone covered by the WRF-based output, except where either the WRF- or RAOB-based sounding ended at a height lower than 20 km AGL. In that situation the comparison ended at the maximum level covered by both soundings. The mean difference (MD), the mean absolute difference (MAD, standard deviation of the differences (SD), and the root mean square difference (RMSD) between the WRF-generated METCMs and ones from the corresponding RAOBs were computed for each zone for all cases for each age of the GFS data, that is, each RAOB is compared to 5 WRF outputs generated using current (day 0), 1-day-old, …, 4-day-old GFS data sets. These terms for the several statistics replaced the more common mean, mean absolute error, standard deviation, and root mean square error, because the WRF-based METCMs were compared with those from RAOB data, not the actual atmosphere. While good approximations, RAOBs are subject to errors arising from, for example, instrument error, balloon drift, and differences from the nominal sounding time.

The differences in those variables for each "age" of GFS were compared in another spreadsheet. Tables were constructed where the values for each variable and zone were compared between various "ages" of GFS. For example, the differences were computed between temperature statistics for WRF-based profiles that used 96–120 h GFS data (RAOB 108 h from start of the GFS data) and WRF-based profiles that used current GFS data (0–24 h, RAOB 12 h from start of the GFS data). Data produced from more recent GFS values were subtracted from the older ones. As a result, positive numbers indicated better values for MAD, SD, and RMSD from the newer GFS data. The MD values may or may not indicate better or worse values. For example, subtracting a small positive or negative value from a larger negative value would result in negative value that would suggest the older GFS was better. The MAD normally is a better indicator of how close the WRF-

based METCMs are to the RAOB-based ones. Tabular and graphical depictions were prepared and several examples are shown in Section 4.

The GTRAJ (v3.9.7) program was provided by ARDEC and is considered a standard for trajectory calculations. As noted in the GTRAJ user's guide, it is a trajectory simulation program that may be run interactively or scripted. The program uses the point mass or modified point mass equations of motion to simulate the trajectory of a projectile in flight. The program uses a database to obtain aerodynamics and ballistics for the selected projectile. There is also aerodynamic data available for miscellaneous shapes such as fragments, cylinders, and cubes. The user may elect to use a custom database instead of the standard one. Frehlich, et al. (2008) describe an earlier version of GTRAJ they employed in their study of the effect of turbulence on ballistic testing procedures.

For each case, the input to GTRAJ includes the METCM from the RAOB; the 5 METCMs from WRF; and the elevation (MSL) of the RAOB site or from the WRF terrain database; latitude (RAOB and WRF have the same value in this study); and firing information such as azimuth (direction) of fire, cannon type, projectile type, and so on. The cannon was a standard 155-mm system with a commonly used projectile fired at an elevation that would produce ranges on the order of 22–24 km with apogees around 7.5 to 8.5 km AGL. The radial distance (RD) is then computed for each instance (e.g., WRF at one GFS "age" for one comparison time for one site for one azimuth). The RD is the distance from the gun to the target, which may be computed from the range and deflection where RD is the square root of the sum of the squares of the range and the deflection. In order to at least partially account for the variation in RD with azimuth, the simulated firings were run for the 4 cardinal directions (north, east, south, and west). For example, wind and density effects could assist or counteract one another leading to larger or smaller RDs for a given firing azimuth.

The output RDs, ranges, and deflections from GTRAJ for the RAOB and the 5 WRF runs (1 for each age of GFS) for the 4 directions of fire are copied into a spreadsheet. Then the values from the runs that used RAOB-based input are compared to those from the runs with WRF-based input to obtain the differences in range and deflection, which are used to calculate RMD. RMD is the square root of the squares of the differences (ΔD) in range and deflection:

$$\mathrm{RMD} = ((\Delta D_r)^2 + (\Delta D_d)^2)^{1/2}, \quad (1)$$

where the subscripts r and d refer to range and deflection, respectively. The mean and median values of the RMDs over the 4 azimuths are computed for each of the 5 GFS ages in terms of meters and percent of the RD (also named % Range).

4. Initial Results: Meteorological

The first set of comparisons was made for the meteorological variables. The emphasis was on the variables in the METCM as well as the derived variables of density and vector wind speed. METCMs were computed from the RAOB and WRF data for each WRF time from start of the GFS as described previously, entered into spreadsheets where the differences were computed for each pair of WRF and coincident RAOB-based soundings, and statistics computed for each of the METCM layers and the surface (line or zone 0). One RAOB for each site and time provided the comparison data for all of the WRF runs for that day and time. For example, the METCM computed from the Wallops Island, Virginia, RAOB for 2016-05-19 at 12 UTC was compared to the WRF-based METCMs for that location and time for all 5 WRF runs (WRF output for 12, 36, …, 108 h from start of the respective GFS run). The sample size or number of pairs for each layer plus the surface ranged from the maximum number of 50 to a lesser number at the highest levels where either the WRF- or RAOB-based sounding failed to reach 20-km AGL. Table 2 shows a sample for wind speed for WRF-based METCMs (i.e., from the WRF simulations using 72- to 96-h GFS data). The WRF was run for 12 h after the start of the selected period, that is, it began at 72 h of GFS model time from the start of the GFS data for day –3.

Table 2 Statistics for wind speed (kn) comparisons where 72- to 96-h GFS data were used for the WRF calculations and compared to the respective lines derived from the coincident RAOBs. WRF-based soundings were obtained for 84 h after the start time of the GFS (0-h GFS forecast). The heights shown have units of meters and are zone midpoints except line 0, which is the surface.

Line	Height	Samples	MD	MAD	SD	RMSD
0	0	50	2.94	4.94	6.33	6.92
1	100	50	3.08	5.92	6.91	7.50
2	350	50	3.38	8.10	10.15	10.60
3	750	50	3.66	7.70	10.20	10.74
4	1,250	50	4.14	7.70	10.30	11.01
5	1,750	50	3.30	7.86	10.85	11.24
6	2,250	50	1.36	7.64	10.60	10.58
7	2,750	50	0.92	7.68	10.59	10.53
8	3,250	50	1.30	7.30	9.90	9.89
9	3,750	50	1.34	6.58	9.22	9.22
10	4,250	50	1.70	7.34	9.97	10.01
11	4,750	50	1.88	8.80	11.75	11.78
12	5,500	50	1.24	9.92	13.33	13.25
13	6,500	50	1.20	11.08	14.70	14.60
14	7,500	50	1.28	11.08	15.24	15.14
15	8,500	50	3.16	10.64	15.24	15.41
16	9,500	50	4.84	10.44	15.72	16.30
17	10,500	50	5.04	10.52	14.93	15.62
18	11,500	50	3.74	8.90	12.59	13.01
19	12,500	49	1.65	7.20	9.91	9.94
20	13,500	49	0.96	6.63	8.68	8.65
21	14,500	49	–0.27	5.24	6.80	6.73
22	15,500	46	–0.26	5.39	6.63	6.56
23	16,500	44	0.75	4.80	6.37	6.34
24	17,500	42	1.83	4.88	6.85	7.02
25	18,500	41	1.24	6.07	7.47	7.48
26	19,500	25	2.20	5.40	6.61	6.84

Tables similar to Table 2 were prepared for the other variables and for the other WRF simulations or runs using GFS data with different forecast start times. WRF simulations are referred to by the GFS forecast time at the verification time. For example, the 108-h WRF run uses GFS data with a 0-h forecast 108 h prior to the RAOB time (96-h prior to the WRF 0-h forecast). Figures 2–6 present graphical representations of those WRF data using the 5 different GFS inputs for vector wind speed, virtual temperature, and density.

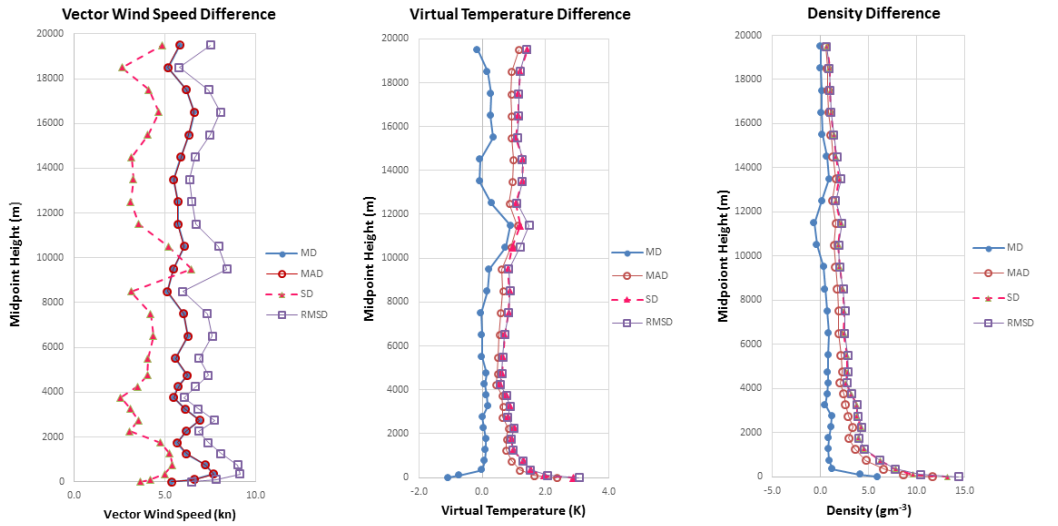

Fig. 2 Graphs showing the 12-h statistics for differences in vector wind speed (kn), virtual temperature (K), and density (gm^{-3})

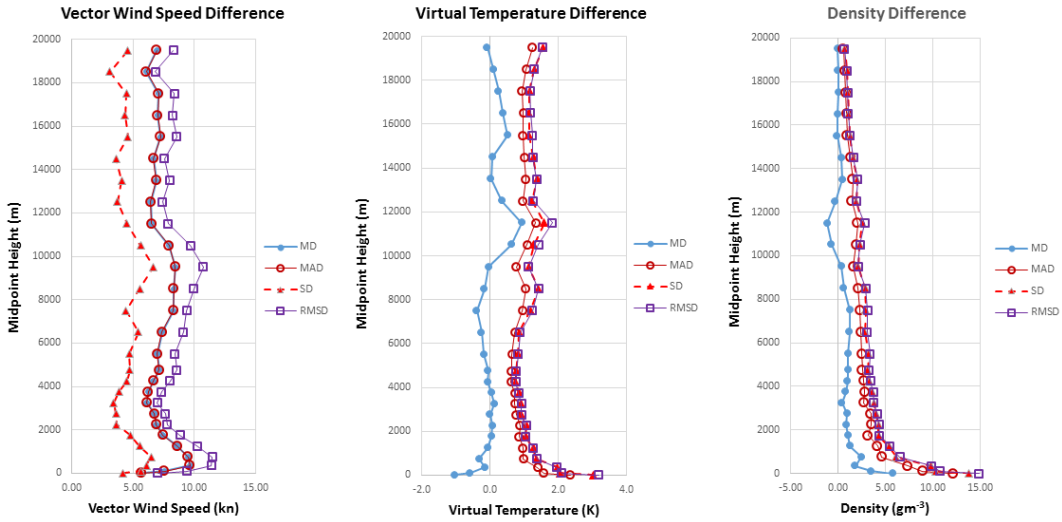

Fig. 3 Graphs showing the 36-h statistics for differences in vector wind speed (kn), virtual temperature (K), and density (gm^{-3})

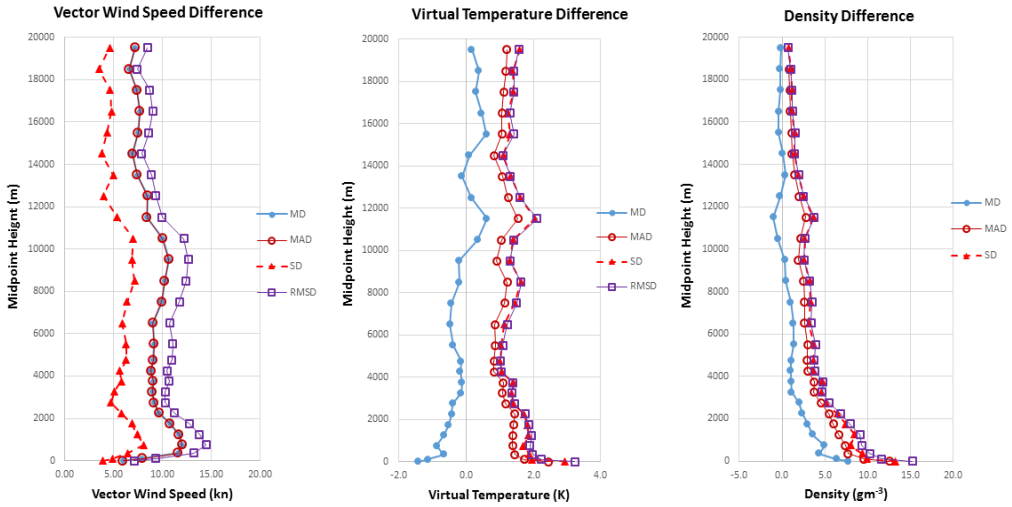

Fig. 4 Graphs showing the 60-h statistics for differences in vector wind speed (kn), virtual temperature (K), and density (gm^{-3})

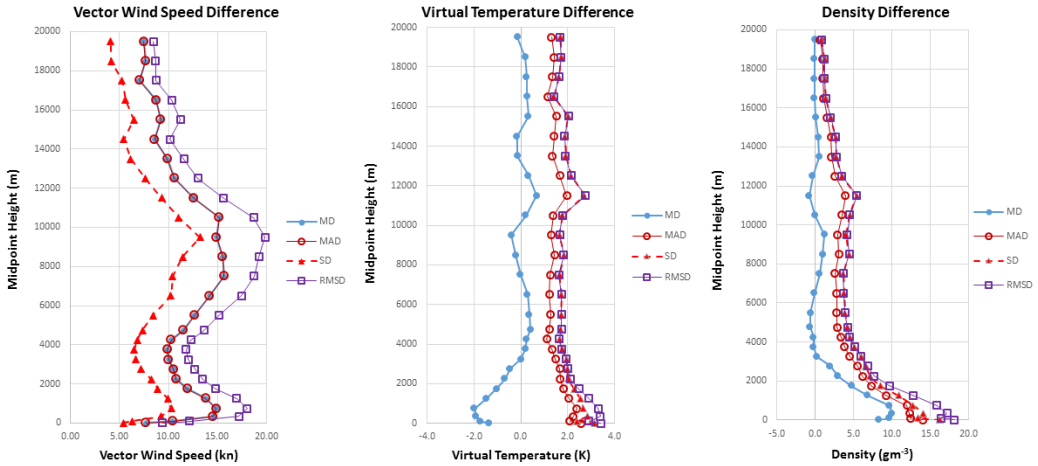

Fig. 5 Graphs showing the 84-h statistics for differences in vector wind speed (kn), virtual temperature (K), and density (gm^{-3})

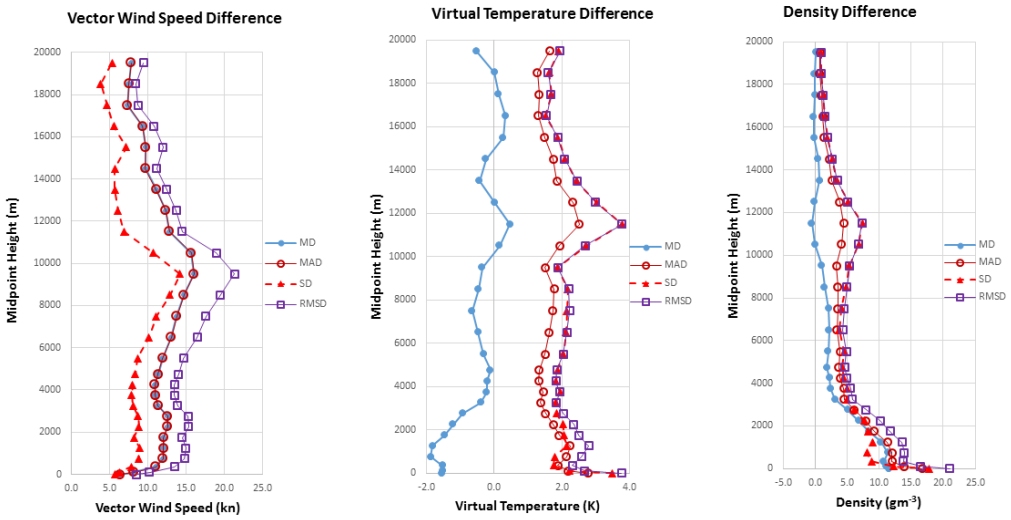

Fig. 6 Graphs showing the 108-h statistics for differences in vector wind speed (kn), virtual temperature (K), and density (gm^{-3})

Table 2 and Figures 2–6 present statistics for each METCM zone that show the differences between METCMs derived from WRF using input from each of the several "aged" GFS data sets and those derived from coincident RAOBs. The following table and graphs have the same type of statistics that illustrate any changes in forecast accuracy as compared to the initial forecast at 12 h from the start of the GFS (0-h GFS forecast). The statistical values for the WRF runs were compared for each variable for each METCM layer for each of the WRF model runs. For example, virtual temperatures for the METCM layers plus the surface that were derived from the 108-h WRF run were compared to the values for the respective layers and surface from the 12-h run.

Table 3 presents a sample for wind speed where values from the 108-h WRF run were compared to those from the 12-h run. The few negative MD values may or may not indicate that the 108-h WRF occasionally led to better outcomes for the reason given earlier, that is, subtracting a positive or negative value from a negative value of a larger magnitude will lead to a negative number. Consequently, the MAD is a better indicator as is the RMSD.

Table 3 Wind speed (kn) differences between comparisons using 96- to 120-h GFS data (108-h WRF run) minus those using 0- to 24-h GFS data (12-h WRF run). Comparisons using WRF-based soundings for 12 h after the start time of the GFS (0-h GFS forecast) were subtracted from comparisons for 108 h after the start time. The heights shown have units of meters and are zone midpoints except line 0 which is the surface.

Line	Height	Samples	MD	MAD	SD	RMSD
0	0	50	0.4	0.6	1.9	1.9
1	100	50	–1.1	0.7	2.1	1.5
2	350	50	–1.2	2.2	3.5	3.1
3	750	50	–0.6	3.3	4.5	4.4
4	1,250	50	0.4	3.1	2.9	2.9
5	1,750	50	2.2	3.3	3.6	3.9
6	2,250	50	1.6	3.6	6.0	6.1
7	2,750	50	1.1	3.9	6.2	6.2
8	3,250	50	1.5	4.1	5.6	5.7
9	3,750	50	1.8	3.7	5.4	5.6
10	4,250	50	1.8	4.0	5.3	5.5
11	4,750	50	1.8	4.0	5.4	5.5
12	5,500	50	1.7	4.3	5.7	5.8
13	6,500	50	1.3	5.1	7.2	7.2
14	7,500	50	0.3	5.8	8.1	8.0
15	8,500	50	1.1	6.8	10.5	10.5
16	9,500	50	2.0	8.0	9.5	9.6
17	10,500	50	2.3	7.5	8.5	8.8
18	11,500	50	0.6	5.7	7.5	7.2
19	12,500	49	–0.8	5.1	5.5	5.1
20	13,500	49	0.2	2.9	3.0	3.0
21	14,500	49	–0.2	1.8	2.1	2.0
22	15,500	46	–0.5	1.2	1.9	1.8
23	16,500	44	–1.1	0.9	1.2	1.1
24	17,500	42	1.3	0.7	0.9	1.1
25	18,500	41	1.1	1.8	2.4	2.5
26	19,500	25	0.7	1.8	1.2	1.4

As with the individual “GFS age” comparisons, the tables also may be presented in graphical form. Figure 7 shows density and related RMSD values, and Fig. 8 presents wind RMSD values. In these figures, the forecast degrades if the values for the older GFS data are larger than for the newer data. For example, the pressure differences in Fig. 7 are greater for the 84-h WRF than for the 60-h WRF runs.

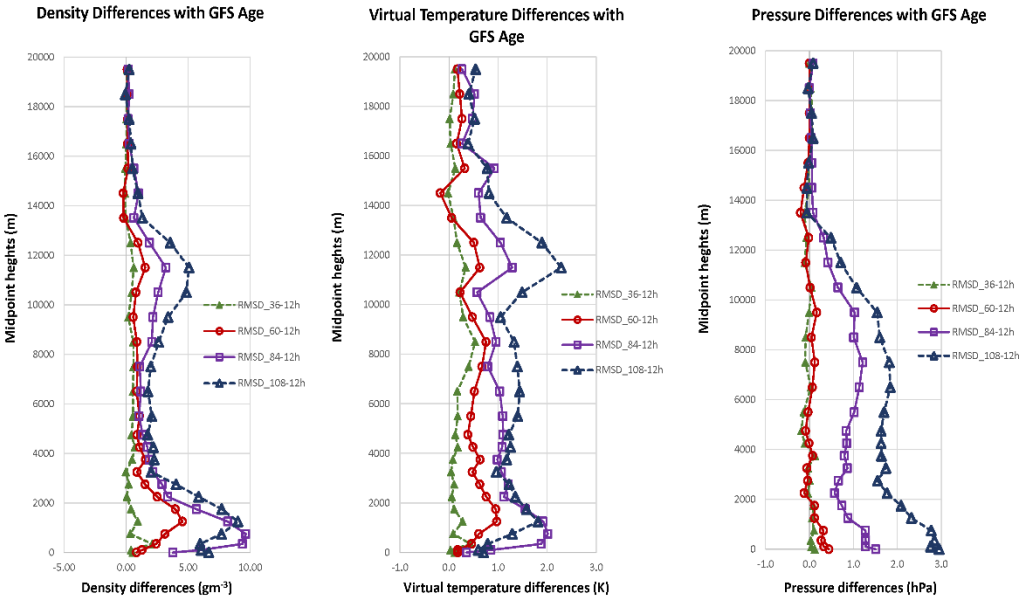

Fig. 7 RMSD differences between the density, virtual temperature, and pressure comparisons for the times shown on the charts. The statistics for the METCMs derived from the 36-, 60-, 84-, and 108-h WRF runs compared to those from the 12-h run are shown for each layer (zones 1–26) plus the surface (zone 0). The midpoints of the layers are in meters AGL.

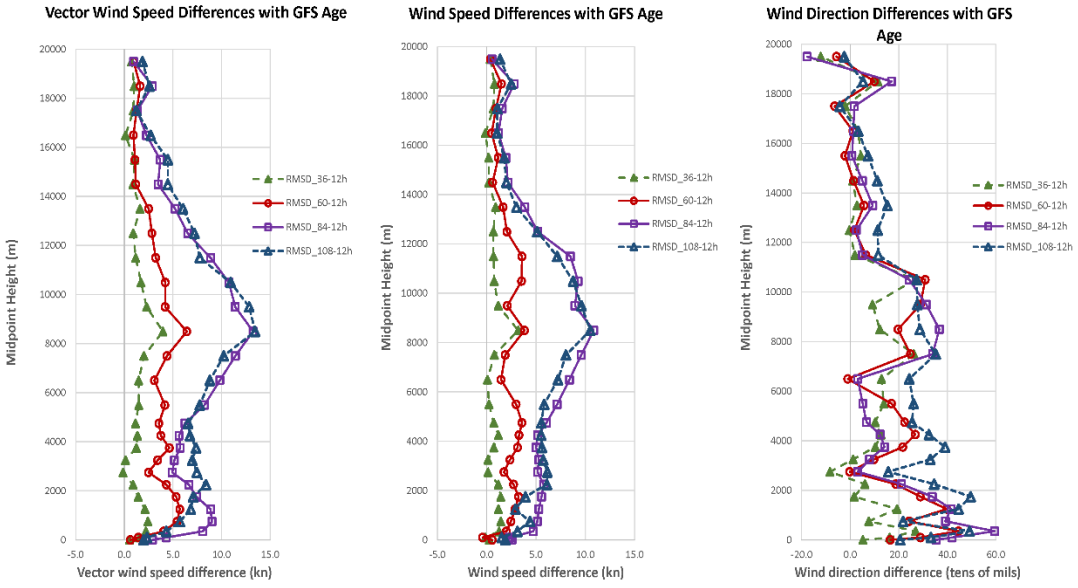

Fig. 8 RMSD differences between the vector wind speed, wind speed, and wind direction comparisons for the times shown on the charts. The statistics for the METCMs derived from the 36-, 60-, 84-, and 108-h WRF runs compared to those from the 12-h run are shown for each layer (zones 1–26) plus the surface (zone 0). The midpoints of the layers are in meters AGL.

In general, the older the GFS input, the greater the RMSD "error" relative to the 12-h WRF-based METCMs. However, occasionally older GFS data appear to provide values closer to the 12-h WRF-based METCMs. Most notably the vector wind speed and the wind speed values for the 108-h WRF-based METCMs for more than a few layers appear closer to the 12-h values than the 84-h values (10 and 15 of 27 zones, respectively). The wind direction differences vary widely though for 19 of 27 zones, including the surface, and the 84-h results are closer to the 12-h values than the 108-h results. For several zones (4,750-, 5,500-, and 6,500-m AGL) the 108-h results are closer than the 36-h wind directions.

5. Initial Results: Trajectories

GTRAJ was employed to compute trajectories using the METCMs from RAOBs and the WRF runs with input from the 5 differently aged GFS data sets. Trajectories computed with METCMs from WRF using GFS data for days 0 through minus 4 were compared with METCMs from coincident RAOBs, as discussed previously. RMD values were computed independently for the 4 cardinal directions so as to have an idea of likely variation with azimuth and consequently to mitigate possible effects that could arise from selecting a single azimuth. A small RMD could occur in one direction of fire if effects of a large density error compensated for a large wind error, but the RMD would most likely be much larger for the opposite azimuth where density and wind errors would reinforce their effects.

The RMDs computed using GTRAJ generally followed the accuracy (i.e., agreement to the coincident RAOBs) of the METCMs derived from the WRF output. Nevertheless, there were major variations in RMD that did not seem to follow the general trend. The following tables provide an indication of the overall trends and the significant variation within those trends. The mean and median values for each GFS age were computed for each site and time where one site and time equals one case (e.g., Anchorage on 2016-04-06 at 12 UTC), where each case has a mean and a median RMD computed from the RMDs for the 4 firing directions for each GFS age. Then the means and medians of the mean and median RMDs of each case were computed for all 50 cases for each GFS age. In addition, the standard deviations of the mean and median values were computed for the 50 cases. The standard deviations provide a measure of the variation within each GFS age category.

Tables 4 and 5 present the means and standard deviations of the mean and median RMDs, respectively, for all sites and times by age of GFS input in terms of meters and percent of RD. The Appendix presents the case-by-case mean and median RMDs. WRF was run for 12 h for the several GFS data sets as indicated in Fig. 1.

For example, WRF ran for 12 h after using the 0- to 12-h GFS forecast, 12 h using the 24- to 36-h GFS forecast from the previous day, and so on through 12 h with the 96- to 108-h GFS forecast from 4 days earlier. For each case, the 5 METCMs derived from WRF were compared with the RAOB-based METCM at 12 h after the 0-h WRF forecast (see Fig. 1).

Table 4 Means, medians, and standard deviations (Std Dev) over the 50 cases of mean RMDs over the 4 firing directions in terms of meters and % RD for the 5 WRF times from start of GFS (0-h GFS forecast)

	WRF times from start of GFS data									
	12 h	**36 h**	**60 h**	**84 h**	**108 h**	**12 h**	**36 h**	**60 h**	**84 h**	**108 h**
	Meters					**% RD**				
Mean	86.8	123.0	182.4	273.5	254.3	0.383	0.543	0.804	1.210	1.122
Median	76.1	103.2	155.7	219.6	184.5	0.334	0.443	0.690	0.971	0.815
Std Dev	53.6	75.3	110.3	207.6	200.7	0.239	0.339	0.492	0.921	0.898

Table 5 Means, medians, and Std Dev over the 50 cases of median RMDs over the 4 firing directions in terms of meters and % RD for the 5 WRF times from start of GFS (0-h GFS forecast)

	WRF times from start of GFS data									
	12 h	**36 h**	**60 h**	**84 h**	**108 h**	**12 h**	**36 h**	**60 h**	**84 h**	**108 h**
	Meters					**% RD**				
Mean	83.7	119.0	176.9	264.6	249.3	0.369	0.526	0.781	1.167	1.104
Median	72.7	98.7	153.9	202.4	179.2	0.311	0.418	0.681	0.907	0.785
Std Dev	52.4	74.2	107.4	200.5	197.1	0.232	0.335	0.482	0.889	0.889

As expected the mean and median values are similar, but not the same, and increased as the GFS input aged from the 12-h through the 84-h computations. However, the mean and median values decreased from the 84-h to the 108-h WRF runs. Since the standard deviation gives a measure of the variation of the RMDs for the 50 cases, the variation appears to peak around the 84-h output with a drop or at least a leveling off afterward at around 108 h. This unexpected result appears to be related to the wind speed and direction improvement noted in Fig. 8.

As suggested by the standard deviations, there is significant variation from case to case in either mean or median RMD for the several WRF times. On a case-by-case basis, the minimum mean and/or median RMD for an earlier time may exceed that for a later time and vice versa for the maximum RMD. For example, the mean RMD for the 36-h WRF-based METCM may be less than that for the 12-h METCM, or the maximum mean RMD for all 5 times may occur for the 60-h METCM. Table 6

presents the number of cases where there was a minimum or maximum value of mean or median RMD for each time (GFS period).

Table 6 Number of occasions for each WRF time from start of GFS where there was a minimum or maximum mean or median value of the RMD, where a single mean or median is for the 4 directions of fire of each case and WRF time

	No. of minimums					No. of maximums				
	12 h	36 h	60 h	84 h	108 h	12 h	36 h	60 h	84 h	108 h
Mean	25	14	8	3	0	0	3	7	23	17
Median	26	12	8	4	0	0	2	8	24	16

As shown in Table 6, the number of minimums or maximums of either mean or median RMDs do not match for all times. That result is not unexpected since the RDs for each simulated firing are different for different METCMs and elevations. In addition, the minimum and maximum values for all 50 cases were extracted for each WRF time category as presented in Table 7.

Table 7 Minimum and maximum mean RMDs for each WRF time (or GFS data age) category. Minimum and maximum values shown on the top and bottom lines, respectively, with values in meters on the left and % RD on the right.

Meters					% RD				
12 h	36 h	60 h	84 h	108 h	12 h	36 h	60 h	84 h	108 h
11.1	27.0	42.7	31.5	38.7	0.047	0.120	0.194	0.129	0.172
288.3	441.4	464.4	844.8	1135.7	1.282	2.006	2.110	3.719	5.088

As expected the maximum values increased with age of GFS data, but not entirely for the minimum values. As shown in Table 7 the largest minimum value occurred for the 60-h WRF run. On the other hand, the largest maximum value occurred for the 108-h run. Table 8 presents the same numbers as Table 7 but for the median RMDs.

Table 8 Minimum and maximum median RMDs for each WRF time (or GFS data age) category. Minimum and maximum values shown on the top and bottom lines, respectively, with values in meters on the left and % RD on the right.

Meters					% RD				
12 h	36 h	60 h	84 h	108 h	12 h	36 h	60 h	84 h	108 h
10.3	30.1	39.0	27.2	36.4	0.044	0.125	0.165	0.110	0.158
288.4	440.8	460.0	835.6	1106.0	1.268	1.989	2.116	3.748	5.033

For the median values, the second smallest minimum in meters and % RD was the one at 84 h though the value in meters was close to that for 36 h. Again, the largest minimum occurred for the 60-h category. The maximum values in Table 8 followed

the same trend as in Table 7 with increasing size as the WRF time from start of GFS increased.

An additional consideration is whether or not the model produces better outcomes than using standard MET. Standard MET is based on the International Civil Aviation Organization 1976 Standard Atmosphere as described in STANAG 4061 (2000). It assumes a standard lapse rate for temperature and pressure, and wind speed is set at 0. Earlier work using live-fire data suggested RMDs relative to RD calculated from RAOB METCMs are on the order of 3% to 4%, occasionally much more or much less. A comparison of 12 cases from this study led to similar results, with averages of mean or median values of 3.9% and 3.5%, respectively. Individual RMDs varied considerably, from as small as 0.68% (PANC on 2016-06-06 at 12 UTC) to as large as 6.47% (VEF on 2016-06-18 at 12 UTC). Both cases also had much larger and smaller RMDs, respectively (3.74% and 2.80 %), suggesting that the effects of wind and density errors augmented or counteracted one another. Table 9 presents the number of times each of the 50 case's mean or median RMD (50 values of each) exceeded 3.5% for each GFS age. The number was the same for both mean and median RMDs.

Table 9 Number of cases where the mean or median RMD of the 4 azimuth directions exceeded 3.5%

	12 h	36 h	60 h	84 h	108 h
Mean	0	0	0	1	1
Median	0	0	0	1	1

Even though there are not enough cases for a definitive statement, it appears that the model-based results should be better than standard MET through the 60-h category. Nevertheless, for one of the cases examined, the value at 60 h slightly exceeded that for standard MET. On the other hand, the largest mean RMD for one case from the use of model data (108-h WRF run) was slightly smaller than that from the use of standard MET (both were slightly higher than 5% RD). As with all similar data sets examined to date, there is wide variation from the mean and median values of Tables 4 and 5, as also suggested in Tables 6–8. Occasionally, standard MET can produce a better outcome than a model-based or RAOB-based METCM for a specified direction of fire even when using relatively recent GFS or other large-scale model input due to cancellation of otherwise large errors in density and wind.

6. Conclusion

This study looked at the potential degradation of WRF-based METCMs relative to RAOBs that served as an approximations to the real atmosphere using differences of meteorological variables and impact points from simulated (GTRAJ) trajectories. In general, the meteorological variables from the WRF-based profiles deviated more from the RAOB-based values as the age of the GFS data increased. However, it appears that the wind estimates slightly improved at many heights as the GFS data aged from 72–84 h to 96–108 h (84- and 108-h WRF output, respectively). While an investigation in depth is beyond the scope of this study, a brief look showed that at least some of the situations leading to unexpected results seemed to arise when the centerline of a trough or a low center lay not far from one or more RAOB sites. A small displacement of the trough or low can lead to a GFS grid point location being on the east or west side of the centerline or center, respectively, or just being closer or further from the centerline or center. The former, in turn, may lead to a southerly wind changing to a northerly wind or vice versa sometimes with a fairly significant wind speed in each direction, and the latter to very different wind speeds even if in a similar direction. Either one could result in a greater difference from the observed RAOB wind. For example, the former situation seems to have occurred over the Alaska sites (Table 1) around 6 April 2016 based on 700-, 500-, and 300-hPa weather charts (not shown, but available at http://archive.atmos.colostate.edu via the included links).

As with the meteorological variables, the GTRAJ results suggested a general degradation with increasing GFS age of the RMDs generated using the WRF-based METCMs relative to those from the RAOB-based METCMs. However, a leveling off or a decrease in the difference between the WRF- and RAOB-based RMDs occurred from the 84- to 108-h comparisons, based on the data used in this report. Also the mean or median values on a case-by-case basis varied widely from one site to another or between the coincident RAOB times for a given site. In future, the variation in results by site and between individual GFS data sets could be investigated when a larger set of additional comparisons become available.

Overall, the data suggest that almost all the time model-based METCMs for artillery simulations outperform standard MET up through a GFS age of 60 h. While the mean differences in mean or median RMD for 84- and 108-h WRF are noticeably smaller than those from the use of standard MET, occasionally standard MET could lead to a better result. Nevertheless, the mean values and the other statistics suggest the use of model-based METCMs is most often preferable than the use of standard MET. If the use of standard MET was to be considered, investigation of more complete models that include latitude, seasonal, and diurnal

variations would be suggested, but that would require additional study to evaluate potential value.

The results of this report suggest that the use of METCMs from WRF-based soundings using large-scale model input without data assimilation can lead to simulated trajectories that are within 1.25% RD on average relative to trajectories calculated using METCMs from RAOB for all WRF times of this report. For WRF times of 60, 36, and 12 h, the mean RMD decreases to about 0.8%, 0.54%, and 0.38% RD, respectively, and a little less for the respective median RMDs. However, the variation from one location and time to another is large and any one RMD may be much smaller or larger. Future research should investigate the relation between individual outcomes and the atmospheric situation, as well as differences by location or region. The use of trajectory calculations from GTRAJ or a similar simulation tool provides a means to assess the integrated or net accuracy of model output spatially over the path of the simulated projectile. The simulated time of flight is often on the order of a minute or 2, and consequently, can provide a nearly "instantaneous" estimate. When possible, use of actual live-fire results can provide an insight into the actual atmosphere not otherwise attainable.

7. References

Cogan J. A generalized method for vertical profiles of mean layer values of meteorological variables. Adelphi (MD): Army Research Laboratory (US); 2015. Report No.: ARL-TR-7434. Available at http://www.arl.army.mil/arlreports/2015/ARL-TR-7434.pdf.

Dutsch ML. Evaluation of the WRF model based on observations made by controlled meteorological balloons in the atmospheric boundary layer of Svalbard. Bergan (Norway): Meteorologisk Institutt; 2012.

Frehlich R, Sharman R, Clough C, Padovani M, Fling K, Boughers W, Walton WS. Effects of Atmospheric Turbulence on Ballistic Testing. J Appl Met Climatol. 2006;47:1539–1549.

Gemmill W, Katz B, Li X. Daily real-time, global sea surface temperature–high resolution analysis: RTG_SST_HR. Camp Springs (MD): The National Center for Environmental Prediction; 2007 Oct. Report No.: 260.

Kilpelainen T, Vihma T, Mannienen M, Sjoblom A, Jakobson E, Palo T, Maturilli M. Modelling the vertical structure of the atmospheric boundary layer over Arctic fjords in Svalbard. Q. J R Met Soc. 2012;138:1867–1883.

Lee JA, Kolczynski WC, McCandless TC, Haupt SE. An objective methodology for configuring and down-selecting an NWP ensemble for low-level wind prediction. Mon Wea Rev. 2012;140:2270–2286.

Reen BP. Army Research Laboratory (US), Adelphi, MD. Personal communication, 2015.

Reen BP, Stauffer DR, Davis KJ. Davis, 2014. Land-surface heterogeneity effects in the planetary boundary layer. Boundary-Layer Met. 2014;150:1–31.

Skamarock WC, Klemp JB, Dudhia J, Gill DO, Barke DM, Duda MG, Huang X-Y, Wang W, Powers JG. A description of the advanced research WRF Version 3. Boulder (CO): National Center for Atmospheric Sciences, Boulder; 2008 Jun. Report No.: NCAR/TN-475+STR.

STANAG 4061. Adoption of a Standard Ballistic Meteorological Message, MET (Edition 4). Washington (DC): North Atlantic Treaty Organization, Military Agency for Standardization; 2000.

INTENTIONALLY LEFT BLANK.

Appendix. Individual Mean and Median Radial Miss Distances (RMDs) per Site

Tables A-1 and A-2 have the individual case mean and median radial miss distances (RMDs) for each site, Weather Research and Forecast (WRF) model time relative to Global Forecast System (GFS) start (0-h forecast), and radiosonde observation (RAOB) (R) date and time used for the comparisons. An individual case value is for the 4 azimuths/directions of fire. There are 50 cases, 5 GFS ages, and 4 trajectory azimuths used in the study. The overall minimum, maximum, mean, median, and standard deviations of the case-by-case values are repeated from Tables 4 and 7, and 5 and 8, respectively, at the bottom of Tables A-1 and A-2 for convenience.

Table A-1 Individual case values of mean RMDs for each WRF time from start of GFS. The region (e.g., Alaska) and comparison RAOB (R) dates and times are shown, and the site codes are listed in the left most column. WMO notations are used when available, otherwise the first 3 or 4 letters of the site's name are used (e.g., MEIN for Meiningen). The values from Tables 7 and 4 are listed at the bottom.

	12 h	36 h	60 h	84 h	108 h	12 h	36 h	60 h	84 h	108 h
			Meters					% RD		
Alaska				R_2016011100						
PADQ	108.8	152.4	434.0	421.8	553.1	0.487	0.686	1.943	1.901	2.466
PAKN	132.3	171.4	119.0	395.4	345.6	0.590	0.766	0.533	1.783	1.544
PANC	115.0	55.2	91.0	453.2	1135.7	0.519	0.248	0.410	2.029	5.088
				R_2016040612						
PADQ	145.6	441.4	464.4	492.8	542.1	0.662	2.006	2.110	2.240	2.463
PAKN	77.8	124.5	42.7	62.1	145.3	0.355	0.568	0.194	0.283	0.661
PANC	72.0	92.0	90.7	110.3	101.8	0.329	0.422	0.416	0.506	0.463
East Coast US				R_2016032300						
GSO	56.9	72.8	44.6	62.1	114.3	0.249	0.316	0.195	0.269	0.496
IAD	30.5	37.2	134.0	53.2	57.7	0.135	0.165	0.597	0.231	0.252
MHX	83.3	73.0	48.7	114.5	203.6	0.371	0.322	0.215	0.507	0.905
RNK	63.7	83.7	53.5	80.3	119.7	0.274	0.358	0.231	0.343	0.509
WAL	53.0	104.9	100.3	51.1	92.4	0.235	0.471	0.453	0.226	0.413

Table A-1 Individual case values of mean RMDs for each WRF time from start of GFS (continued).

	12 h	36 h	60 h	84 h	108 h	12 h	36 h	60 h	84 h	108 h
			Meters					% RD		
East Coast US				R_2016051912						
GSO	134.9	62.5	228.2	303.3	366.0	0.589	0.269	0.991	1.330	1.585
IAD	28.1	190.9	371.9	257.4	613.8	0.126	0.848	1.639	1.150	2.720
MHX	29.3	100.0	172.1	271.2	214.0	0.131	0.443	0.764	1.197	0.946
RNK	95.5	197.8	399.3	639.7	559.4	0.408	0.844	1.694	2.755	2.384
WAL	24.4	226.3	333.7	469.0	473.5	0.110	1.006	1.465	2.088	2.090
Midwest US				R_2016010212						
AMA	66.1	101.5	253.0	389.5	265.7	0.281	0.430	1.069	1.648	1.125
DDC	25.1	171.8	210.2	223.8	134.9	0.109	0.741	0.906	0.963	0.575
LMN	41.7	154.3	230.7	183.8	208.5	0.185	0.684	1.019	0.807	0.916
OUN	101.9	84.4	143.1	267.4	122.9	0.450	0.373	0.629	1.185	0.550
TOP	288.3	196.8	151.1	346.9	339.6	1.282	0.874	0.673	1.545	1.506
				R_2016021012						
AMA	45.3	40.0	85.4	126.0	117.6	0.191	0.168	0.360	0.534	0.494
DDC	97.8	120.8	66.6	130.3	139.3	0.421	0.519	0.281	0.576	0.601
LMN	25.5	94.9	77.1	157.6	38.7	0.116	0.423	0.347	0.716	0.172
OUN	88.0	89.8	93.4	122.2	128.1	0.391	0.402	0.415	0.551	0.567
TOP	58.0	27.0	174.4	177.5	50.8	0.253	0.120	0.787	0.818	0.229

Table A-1 Individual case values of mean RMDs for each WRF time from start of GFS (continued).

	12 h	36 h	60 h	84 h	108 h	12 h	36 h	60 h	84 h	108 h
	Meters					% RD				
Southwest US				R_2016061812						
FGZ	79.6	127.1	126.9	141.7	152.0	0.310	0.496	0.495	0.554	0.594
NKX	52.2	50.3	134.6	149.3	150.4	0.227	0.218	0.586	0.650	0.655
PHX	11.1	57.4	87.3	138.8	123.4	0.047	0.246	0.374	0.594	0.528
TUS	62.4	105.7	183.5	212.7	185.6	0.262	0.444	0.771	0.893	0.779
VEF	83.6	116.1	75.6	48.8	103.2	0.353	0.491	0.320	0.205	0.436
Australia				R_2016050512						
YMML	61.6	61.5	123.8	73.6	98.7	0.272	0.272	0.547	0.325	0.438
YPAD	59.5	50.2	100.6	148.9	168.1	0.265	0.224	0.448	0.662	0.747
Germany				R_2016020700						
ETGB	199.0	140.6	169.8	718.1	356.4	0.891	0.632	0.762	3.210	1.611
ETGI	61.0	135.1	217.9	844.8	236.3	0.270	0.597	0.959	3.719	1.056
ETGK	90.9	150.5	151.5	471.0	367.5	0.402	0.664	0.668	2.073	1.626
MEIN	142.6	167.3	283.0	785.1	463.5	0.626	0.736	1.244	3.446	2.044
STUT	163.4	203.5	258.7	743.9	437.2	0.724	0.902	1.146	3.306	1.947
				R_2016030700						
ETGB	74.4	174.5	425.2	331.1	280.6	0.338	0.793	1.935	1.505	1.276
ETGI	110.9	47.8	199.0	454.6	65.7	0.495	0.213	0.889	2.036	0.295
ETGK	129.6	59.2	283.8	227.2	563.6	0.582	0.262	1.268	1.028	2.547
MEIN	91.4	240.7	295.3	496.9	374.7	0.412	1.075	1.314	2.224	1.664
STUT	61.9	88.6	168.9	215.5	181.4	0.281	0.401	0.757	0.979	0.818

Table A-1 Individual case values of mean RMDs for each WRF time from start of GFS (continued).

	12 h	36 h	60 h	84 h	108 h	12 h	36 h	60 h	84 h	108 h
	Meters					% RD				
South Africa				R_2016050600						
FAIR	32.6	31.4	68.1	31.5	270.5	0.132	0.128	0.278	0.129	1.101
FALE	110.7	69.7	111.9	225.1	139.3	0.491	0.309	0.497	0.998	0.616
South Korea				R_2015110712						
CHEJ	231.3	240.0	282.6	87.8	112.5	1.017	1.051	1.239	0.381	0.486
HEUK	56.3	79.8	159.9	229.5	183.5	0.249	0.351	0.707	1.015	0.811
POHA	66.1	158.6	287.2	227.1	200.4	0.294	0.705	1.272	1.006	0.886
RKJJ	110.6	85.4	232.7	181.6	111.2	0.489	0.373	1.029	0.805	0.492
RKSO	108.1	241.6	77.4	128.7	206.7	0.476	1.070	0.345	0.571	0.918
Min	11.1	27.0	42.7	31.5	38.7	0.047	0.120	0.194	0.129	0.172
Max	288.3	441.4	464.4	844.8	1135.7	1.282	2.006	2.110	3.719	5.088
Mean	86.8	123.0	182.4	273.5	254.3	0.383	0.543	0.804	1.210	1.122
Median	76.1	103.2	155.7	219.6	184.5	0.334	0.443	0.690	0.971	0.815
Std Dev	53.6	75.3	110.3	207.6	200.7	0.239	0.339	0.492	0.921	0.898

Table A-2 Individual case values of median RMDs for each WRF time from start of GFS. The region (e.g., Alaska) and comparison RAOB (R) dates and times are shown, and the site codes are listed in the left most column. WMO notations are used when available, otherwise the first 3 or 4 letters of the site's name are used (e.g., MEIN for Meiningen). The values from Tables 8 and 5 are listed at the bottom.

	12 h	36 h	60 h	84 h	108 h	12 h	36 h	60 h	84 h	108 h
			Meters					% RD		
Alaska				R_2016011100						
PADQ	115.6	142.9	407.5	424.4	538.0	0.499	0.616	1.896	1.903	2.438
PAKN	111.8	143.6	93.3	385.2	330.6	0.500	0.647	0.433	1.683	1.489
PANC	116.3	49.7	89.7	444.8	1106.0	0.516	0.234	0.419	2.013	5.033
				R_2016040612						
PADQ	146.0	440.8	460.0	491.2	538.6	0.656	1.989	2.116	2.205	2.469
PAKN	76.6	125.9	42.1	61.7	134.6	0.350	0.577	0.191	0.281	0.613
PANC	62.9	82.8	92.4	99.4	109.5	0.286	0.377	0.424	0.454	0.500
East Coast US				R_2016032300						
GSO	51.7	76.2	39.0	64.7	97.8	0.236	0.320	0.165	0.272	0.444
IAD	32.2	33.3	128.4	40.2	55.6	0.149	0.143	0.597	0.180	0.254
MHX	79.1	66.0	44.4	108.0	181.1	0.364	0.297	0.202	0.492	0.841
RNK	59.3	87.7	53.0	76.9	113.8	0.266	0.364	0.229	0.318	0.492
WAL	54.0	89.2	100.8	50.8	82.4	0.231	0.387	0.462	0.221	0.363

Table A-2 Individual case values of median RMDs for each WRF time from start of GFS (continued).

	12 h	36 h	60 h	84 h	108 h	12 h	36 h	60 h	84 h	108 h
			Meters					% RD		
East Coast US				R_2016051912						
GSO	127.2	63.7	191.1	307.6	351.4	0.581	0.269	0.810	1.302	1.565
IAD	29.7	180.2	356.4	251.1	619.0	0.127	0.845	1.619	1.168	2.675
MHX	28.7	99.9	154.8	261.8	177.2	0.126	0.432	0.694	1.192	0.787
RNK	87.4	198.1	400.2	647.2	536.8	0.394	0.849	1.658	2.676	2.343
WAL	23.0	219.0	317.8	458.5	462.5	0.098	1.019	1.437	2.097	1.993
Midwest US				R_2016010212						
AMA	65.7	101.4	244.8	369.9	235.3	0.283	0.428	1.065	1.573	1.011
DDC	27.2	170.7	213.4	219.6	128.9	0.114	0.738	0.903	0.973	0.561
LMN	39.6	142.7	227.6	186.9	211.7	0.176	0.645	1.027	0.804	0.925
OUN	99.1	79.3	136.3	255.5	122.9	0.451	0.356	0.613	1.147	0.536
TOP	288.4	191.3	140.5	314.8	297.8	1.268	0.845	0.631	1.384	1.335
				R_2016021012						
AMA	44.8	41.2	79.2	119.5	120.8	0.183	0.168	0.345	0.497	0.493
DDC	96.3	118.7	68.8	119.1	144.0	0.393	0.517	0.287	0.534	0.649
LMN	25.3	90.7	82.7	150.6	36.4	0.113	0.379	0.369	0.688	0.158
OUN	81.8	88.7	89.5	126.6	129.5	0.363	0.391	0.386	0.570	0.568
TOP	53.4	30.1	180.5	199.6	51.8	0.230	0.125	0.791	0.902	0.230

Table A-2 Individual case values of median RMDs for each WRF time from start of GFS (continued).

	12 h	36 h	60 h	84 h	108 h	12 h	36 h	60 h	84 h	108 h
			Meters					% RD		
Southwest US				R_2016061812						
FGZ	75.5	125.6	126.1	137.7	151.8	0.302	0.503	0.504	0.537	0.594
NKX	49.9	50.7	136.0	150.8	152.0	0.212	0.215	0.576	0.638	0.645
PHX	10.3	53.9	84.4	133.3	122.6	0.044	0.230	0.358	0.566	0.521
TUS	56.6	97.5	176.1	204.3	183.5	0.237	0.407	0.736	0.850	0.764
VEF	84.5	115.3	78.4	47.8	101.5	0.348	0.498	0.329	0.201	0.443
Australia				R_2016050512						
YMML	57.5	59.0	125.4	74.0	97.7	0.266	0.273	0.531	0.324	0.435
YPAD	57.1	48.8	100.7	143.1	164.8	0.257	0.219	0.462	0.656	0.749
Germany				R_2016020700						
ETGB	194.0	139.2	168.3	708.5	352.1	0.897	0.618	0.743	3.214	1.562
ETGI	66.1	137.6	214.6	835.6	238.2	0.302	0.606	0.962	3.748	1.064
ETGK	88.0	146.5	153.0	453.7	374.5	0.387	0.641	0.669	2.020	1.650
MEIN	133.7	165.2	286.4	766.3	453.2	0.575	0.730	1.267	3.341	2.018
STUT	150.8	191.8	258.5	611.4	438.4	0.652	0.843	1.138	2.649	1.942
				R_2016030700						
ETGB	69.9	164.3	402.2	294.9	281.1	0.319	0.745	1.818	1.332	1.282
ETGI	89.1	55.7	181.4	457.3	67.8	0.403	0.248	0.809	2.019	0.307
ETGK	127.1	53.2	265.5	220.7	576.1	0.568	0.241	1.143	1.000	2.582
MEIN	91.6	243.9	291.8	492.4	368.5	0.411	1.083	1.258	2.208	1.662
STUT	62.9	73.5	176.4	200.6	183.7	0.285	0.332	0.796	0.912	0.825

Table A-2 Individual case values of median RMDs for each WRF time from start of GFS (continued).

	12 h	36 h	60 h	84 h	108 h	12 h	36 h	60 h	84 h	108 h
			Meters					% RD		
South Africa				R_2016050600						
FAIR	33.8	37.4	60.7	27.2	255.9	0.138	0.155	0.246	0.110	1.059
FALE	98.7	72.8	101.7	178.4	127.8	0.437	0.321	0.451	0.789	0.553
South Korea				R_2015110712						
CHEJ	228.7	221.2	280.1	89.7	119.3	0.986	1.013	1.190	0.381	0.510
HEUK	58.1	59.7	162.0	220.1	175.0	0.250	0.270	0.725	0.944	0.783
POHA	59.2	157.8	282.7	227.8	238.3	0.256	0.697	1.281	1.008	1.043
RKJJ	111.9	83.6	230.7	179.7	113.8	0.486	0.373	1.002	0.774	0.507
RKSO	108.8	243.0	66.9	136.9	213.8	0.478	1.058	0.289	0.592	0.924
Min	10.3	30.1	39.0	27.2	36.4	0.044	0.125	0.165	0.110	0.158
Max	288.4	440.8	460.0	835.6	1106.0	1.268	1.989	2.116	3.748	5.033
Mean	83.738	119.023	176.881	264.553	249.313	0.526	0.781	1.167	1.104	Mean
Median	72.688	98.703	153.905	202.432	179.173	0.418	0.681	0.907	0.785	Median
Std Dev	52.445	74.236	107.367	200.528	197.122	0.335	0.482	0.889	0.889	Std Dev

List of Symbols, Abbreviations, and Acronyms

AGL	above ground level
ARDEC	Armaments Research Development and Engineering Center
ECMWF	European Centre for Medium-Range Weather Forecasting
ESRL	Earth System Research Laboratory
GFS	Global Forecast System
GTRAJ	General Trajectory
IMS	Ice Mapping System
MAD	mean absolute difference
MD	mean difference
METCM	computer meteorological message
MSL	mean sea level
NCEP	The National Center for Environmental Prediction
NCL	NCAR Command Language
NCAR	National Center for Atmospheric Research
NOAA	National Oceanic and Atmospheric Administration
NOHRSC	National Operational Hydrologic Remote Sensing Center
RAOB	radiosonde observation
RD	radial distance
RMD	radial miss distance
RMSD	root mean square difference
SD	standard deviation
UTC	Coordinated Universal Time
WRF	Weather Research and Forecasting
WMO	World Meteorological Organization

1 DEFENSE TECHNICAL
(PDF) INFORMATION CTR
DTIC OCA

2 DIRECTOR
(PDF) US ARMY RSRCH LAB
RDRL CIO LL
RDRL IMAL HRA RECORDS MGMT

1 DIRECTOR
(PDF) US ARMY RSRCH LAB
RDRL CIE
J L COGAN